

Electronic Spectra (Experimental and Simulated), and DFT Investigation of NLO, FMO, NBO, and MESP Characteristics of Some Biphenylcarboxaldehydes

K. Srishailam, L. Ravindranath, B. Venkatram Reddy & G. Ramana Rao

To cite this article: K. Srishailam, L. Ravindranath, B. Venkatram Reddy & G. Ramana Rao (2022): Electronic Spectra (Experimental and Simulated), and DFT Investigation of NLO, FMO, NBO, and MESP Characteristics of Some Biphenylcarboxaldehydes, Polycyclic Aromatic Compounds, DOI: [10.1080/10406638.2022.2130376](https://doi.org/10.1080/10406638.2022.2130376)

To link to this article: <https://doi.org/10.1080/10406638.2022.2130376>

 View supplementary material 

 Published online: 11 Oct 2022.

 Submit your article to this journal 

 View related articles 

 View Crossmark data 



Electronic Spectra (Experimental and Simulated), and DFT Investigation of NLO, FMO, NBO, and MESP Characteristics of Some Biphenylcarboxaldehydes

K. Srishailam^{a,b}, L. Ravindranath^{b,c}, B. Venkatram Reddy^b , and G. Ramana Rao^b

^aDepartment of Physics, SR University Warangal, Warangal, India; ^bDepartment of Physics, Kakatiya University, Warangal, India; ^cDepartment of Physics, Malla Reddy Engineering College, Hyderabad, India

ABSTRACT

Experimental UV–Visible spectral data for biphenyl-4-carboxaldehyde (B4A), biphenyl-3-carboxaldehyde (B3A), and biphenyl-2-carboxaldehyde (B2A) were obtained in the spectral space 200–400 nm in a solution of CDCl_3 . In order to substantiate the experimental data, theoretical quantum chemical calculations were made using time-dependent DFT (TD-DFT) formalism employing B3LYP functional in combination with 6–311++G(d,p) for the three molecules in CDCl_3 solution phase. Certain global reactivity descriptors were evaluated with the highest occupied molecular orbital (HOMO) and lowest unoccupied molecular orbital (LUMO) (FMOs) analysis, with in the frame work of DFT/B3LYP/6–311++G(d,p) method for the three molecules being investigated. The non-linear optical (NLO) material profiles of the three molecules consisting of their static NLO parameters were theoretically investigated to find their utility for NLO applications. Hyperconjugative interactions, as revealed by natural bond orbital (NBO) analysis, helped to explain NLO behavior of the molecules in terms of intramolecular charge transfer (ICT). The reactive sites of B4A, B3A, and B2A molecules were probed by MESP surface analysis.

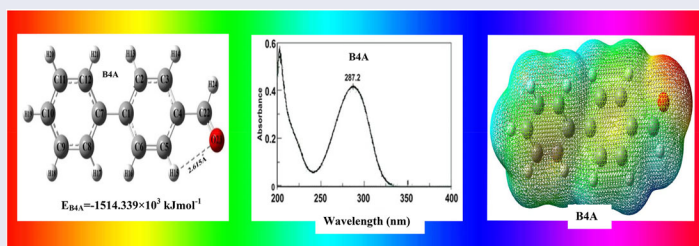
ARTICLE HISTORY

Received 1 July 2022

Accepted 25 September 2022

KEYWORDS

Biphenylcarboxaldehyde; electronic spectra; NLO; FMO; NBO; MESP; DFT



HIGHLIGHTS

- Experimental and simulated electronic absorption maxima agree well for, B4A, B3A, and B2A.
- Highest occupied molecular orbital (HOMO) and lowest unoccupied molecular orbital (LUMO) orbitals are used to understand $\pi \rightarrow \pi^*$ UV–Visible transitions in the three molecules.
- The molecules are highly reactive and stable.
- B4A and B3A are good for developing NLO materials.
- Space around oxygen atom of the aldehyde moiety of the molecules is the most favorable site, for electrophilic attack.

CONTACT B. Venkatram Reddy  bvreddy67@yahoo.com  Department of Physics, Kakatiya University, Warangal 506009, Telangana, India

 Supplemental data for this article can be accessed online at <https://doi.org/10.1080/10406638.2022.2130376>

1. Introduction

Substituted Biphenyls (BP) are known for their importance in commercial applications of liquid crystals,¹ in pharmaceutical research for obtaining high success rates² (e.g. sartan family of drugs used to treat hypertension³) as industrial flame retardants and plasticizers⁴ (e.g. polychlorinated BP and polybrominated BP), and in asymmetric synthesis⁵ of vital chiral ligands^{6,7} (e.g. BINAP and Meo-BIPHEP). Further, the biphenyl moiety plays a pivotal role in imparting biological activity to numerous natural products^{8,9} (e.g. michellamine, steganon, and vancomycin). Moreover, there is an interesting aspect of structure of biphenyl derivatives. The torsional angle around C–C inter-ring bond, associated barrier to internal rotation, and consequent conformer are dictated by two opposing interactions: the π -electron conjugation (i.e. delocalization of π -electrons) between the two phenyl rings favoring a coplanar structure, whereas the repulsion between ortho atoms favoring a non-coplanar conformer. This stimulated intense experimental and theoretical research activity of biphenyl derivatives in order to understand their equilibrium geometries, vibrational frequencies, molecular force field, chemical reactivity, barrier to internal rotation around inter-ring C–C bond, electronic structure, laser-induced fluorescence spectra, and electronic spectra. However, these studies are mainly restricted to methyl-,¹⁰ fluoro-,^{11,12} chloro-,^{13,14} bromo-,¹⁴ amino-,¹⁵ cyano-,¹⁶ and hydroxyl-,¹³ substituted BP. Hence in an earlier article we reported results of our investigation of biphenyl-4-carboxaldehyde (B4A), biphenyl-3-carboxaldehyde (B3A), and biphenyl-2-carboxaldehyde (B2A) involving their torsional potentials, hindered rotation, molecular structure and vibrational properties.¹⁷ As a continuation of this work we report results of our work on B4A, B3A, and B2A covering their UV–Vis spectra (both experimental and simulated), frontier molecular orbital (FMO) characteristics, non-linear optical (NLO) properties, natural bond orbital (NBO) behavior, and molecular electrostatic potentials (MEP). In a recent article, we reported results of such investigations on a couple of thiosemicarbazones.¹⁸ This work is of current interest, as several research articles are published in the immediate recent past, that deal with subject matter of this article, for a good number of other molecular systems.^{19–22}

2. Measurement of spectra

High purity samples of B4A (solid) and B3A (liquid) were purchased from Tokyo Kasei Kogyo Co., Ltd, Tokyo, Japan, whereas B2A (liquid) was procured from Aldrich Chemical Company, St. Louis, MO. They were used as such, without further purification for recording the spectra.

UV–Vis spectra of the three compounds were measured, in a solution of Deuterated Chloroform (CDCl_3), employing Perkin-Elmer UV–Vis LAMBDA-25 double beam spectrometer, in the spectral range 200–400 nm, at room temperature.

3. Computational aspects

In order to evaluate various molecular properties related to electronic transitions, FMO behavior, nonlinear optical parameters, NBO characteristics, and MESPs of B4A, B3A, and B2A, we used *ab initio* quantum chemical calculations modified to include density functional theory (DFT) formalism as available in Gaussian 09/DFT program package.²³ The level of theoretical formalism used consisted of three essential components: (i) Beck's non-local gradient three parameter hybrid exchange functional (B3),²⁴ (ii) Lee–Yang–Parr gradient corrected correlation functional (LYP),²⁵ and (iii) split valence triple zeta basis set, 6–311++G(d,p). We call this B3LYP/6–311++G(d,p) formalism or method.

Time dependent-DFT (TD-DFT) was employed, using the formalism mentioned in the preceding paragraph, to compute electronic absorption spectra of B4A, B3A, and B2A in a solution of CDCl_3 (this is the solvent used to measure experimental spectra).^{26–28}

Orbital energy gap (ΔE), ionization potential (I), electron affinity (A), global chemical hardness (η), global chemical softness (ζ), electronegativity (χ) chemical potential (μ), global electrophilicity index (ω), and maximum charge transfer index (ΔN_{max}) are chemically important parameters. Following common practice, we evaluated ΔE , I, A, η , ζ , μ , ω , and ΔN_{max} for B4A, B3A and B2A, using the highest occupied molecular orbital (HOMO) and lowest unoccupied molecular orbital (LUMO) energies E_{HOMO} and E_{LUMO} , respectively. HOMO and LUMO are called FMOs. Relevant expressions required for calculating above parameters using DFT were taken from literature.^{22,29–31}

Nonlinear optical behavior of a given compound is usually analyzed in terms of its total molecular dipole moment (μ_t) and its components, total molecular polarizability (α_t) and its components, anisotropy of polarizability ($\Delta\alpha$), and first-order static hyperpolarizability (β_i). Their values were found, for B4A, B3A, and B2A, utilizing DFT in conjunction with Buckingham's definitions³² based on finite field approach (see²¹ also for fundamental equations of NLO).

A major structural aspect of B4A, B3A, and B2A is the π -electron conjugation (i.e. delocalization or hyper conjugation) between the two phenyl rings as stated earlier in the introduction. It is essential to quantify this aspect in the three molecules under investigation. This leads to an understanding of several second-order interactions involving occupied orbitals of one subsystem and vacant orbitals of another subsystem. This is achieved by evaluating donor–acceptor interactions for each of the three molecules B4A, B3A, and B2A by subjecting their Fock matrices in NBO basis to second-order perturbation analysis. These interactions reveal themselves as a loss of occupancy from the localized NBO of the idealized Lewis structure into an empty non-Lewis orbital. We used NBO version 3.1 computer program (Madison, UK)³³ which is a part of the Gaussian 09/DFT suit of programs.

MESP $V(\mathbf{r})$ at any point \mathbf{r} (x, y, z) is given exactly by the following expression.^{21,34}

$$V(\mathbf{r}) = \sum_A \frac{Z_A}{|\mathbf{R}_A - \mathbf{r}|} - \int \frac{\rho(\mathbf{r}') d\mathbf{r}'}{|\mathbf{r}' - \mathbf{r}|}$$

where Z_A , \mathbf{R}_A , \mathbf{r}' , \mathbf{r} and $\rho(\mathbf{r}')$ are

Nuclear charge on the nucleus A, position of nucleus A, position of an electron in the molecule, position of a point where $V(\mathbf{r})$ is required in the surroundings of the molecule, and $\rho(\mathbf{r}')$ is electron density (ED) function at the point \mathbf{r}' , respectively. \mathbf{R}_A , \mathbf{r}' , and \mathbf{r} are measured from an arbitrary origin.

The first term on the right-hand side of the above equation represents nuclear contribution to the potential, which is responsible for the positive interaction energy. This arises from the interaction of nuclei belonging to the molecule with a positive test charge situated at \mathbf{r} . The second term in the equation is due to electrons, which is the origin of the negative interaction energy. This energy originates from the interaction of electrons with the same test charge used above at \mathbf{r} . To evaluate MESP, we mapped MESP $V(\mathbf{r})$ onto iso-ED surface. MESP surfaces of B4A, B3A, and B2A are evaluated, along with total ED, using DFT/B3LYP/6–311++G(d,p) level of theory, by mapping MESP onto iso-ED surfaces.

4. Results and discussion

4.1. Frontier molecular orbital (FMO) characteristics

In this section, we wish to present FMOs (i.e. HOMO and LUMO) and their utility to understand UV–Visible spectra and chemical reactivity. FMOs are very important in quantum chemistry for

determination, understanding, and interpretation of a host of molecular electronic and electrical parameters, electronic transitions responsible for absorption bands in UV–Visible region, chemical reactivity of conjugated molecules at molecular level and charge transfer within molecular systems.^{21,22,30,31,35–39}

HOMO can be thought of as an electron donor, whereas LUMO can be considered as an electron acceptor.

4.1.1. UV–Visible spectrum

It is a common practice to employ UV–Visible absorption spectra for quantitative analysis of organic compounds in a solution. But it is almost impossible to avoid impurities in the solution in an organic synthesis. Two methods are available to make quantitative analysis of such a solution possible. The first method requires separation of various impurities present in the solution, whereas the second procedure needs re-synthesis of the impurities separately. Both procedures require considerable time, in addition to being financially taxing. Hence, one should look for an alternative method that can address this problem effectively. The answer is available in numerous theoretical methods, that have the common purpose of simulating UV–Visible spectra. Recently Parrish et al.⁴⁰ reviewed these methods alongwith DFT, wherein they extended variational quantum eigensolver method for calculating electronic transitions. We prefer to use time-dependent DFT (TD-DFT) for this purpose, as it was established that TD-DFT simulates UV–Visible spectra with fair degree of accuracy.^{26–28} Further, such usage conforms to the general purpose of this article.

It is customary to use a three-step procedure^{41,42} to generate UV–Visible spectra theoretically. In the first step, the ground state geometry is optimized until the default convergence limit (i.e. the root-mean-square of forces is less than 3.0×10^{-4} a.u.) is reached. This is followed by the second step, wherein vibrational wave numbers are determined analytically to check for the absence of negative frequencies in order to ensure that the structure corresponds to an actual minimum. In the final step vertical transitions to valence excited states are calculated. In the first two steps, the DFT formalism is employed, while the last step is implemented with its time-dependent variant, i.e. TD-DFT. Optimized molecular geometry of B4A, B3A, and B2A as obtained by implementing the first two steps and reported in our earlier publication,¹⁷ is shown in [Figure 1](#), since the geometry is essential for the computations reported in this article.

Quantum theoretical formalisms described above give rise to a line spectrum for the UV–Visible transitions. This needs to be modified as the corresponding experimental spectrum has a broad shape due to line-broadening effects such as natural line width, Doppler effect, pressure broadening, and thermal excitement. Therefore, each computed line has to be widened to have a Gaussian shape.^{43,44} To realize this, computation of UV–Visible transitions has to be made following an integrated approach.⁴⁵ The input in this process is the electronic transitions generated by TD-DFT. Then, each line spectrum is modified into a Gaussian function making independent optimization by using a convenient value for full width at half maximum (FWHM). This process leads to improved agreement between measured and computed spectra.⁴⁵ It is important to note that there should be certain amount of deviation between the observed and computed values of UV–Visible spectra as it is not possible to incorporate line-broadening effects exactly using present theoretical methods.

Simulated electronic absorption spectral parameters were obtained for B4A, B3A, and B2A in a solution of CDCl_3 using foregoing quantum chemical methods. Solvent effects were addressed by means of polarizable continuum model (PCM). For this, we employed a variant of integrated equation formalism (IEF-PCM),⁴⁶ incorporated into Gaussian version 09 program package.

Measured UV–Visible absorption bands caused by electronic transitions are made available in [Figure 2](#), for B4A, B3A, and B2A. Comparison of these transitions with their corresponding computed parameters can be found in [Table 1](#).

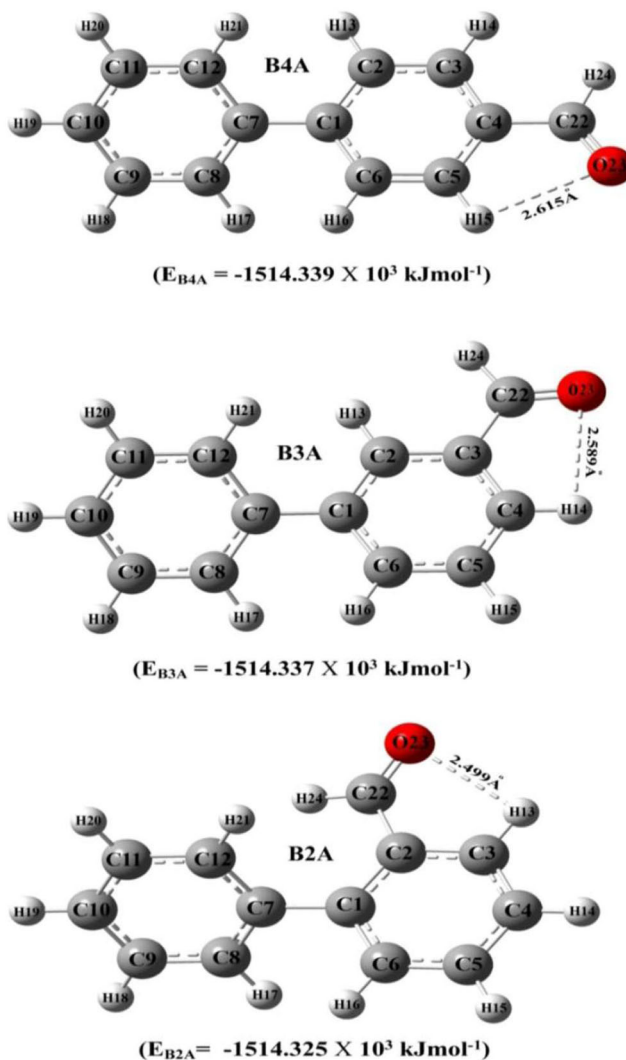


Figure 1. Optimized molecular structure of B4A, B3A, and B2A monomers along with numbering of atoms and intramolecular hydrogen bonding.

According to our calculations B4A, B3A, and B2A should have one electronic transition each, at $\lambda_{\text{max}} = 308.2, 315.8, \text{ and } 302.4 \text{ nm}$, respectively, with corresponding oscillator strength 0.670, 0.031, and 0.103. These are in good agreement with observed electronic transitions near 287.2, 303.1, and 299.9 nm, for B4A, B3A, and B2A, respectively. Prominent HOMO–LUMO and their neighboring molecular orbitals in various electronic transitions are shown in Figure 3, for B4A, B3A, and B2A. Our simulations establish that the experimental bands mentioned in the foregoing paragraph, arise mainly due to H→L transitions (H and L denote HOMO and LUMO, respectively). The percentage contribution of H→L transition is 98%, 88%, and 56% in B4A, B3A, and B2A, respectively. We can attribute H→L electronic transition to $\pi \rightarrow \pi^*$ excitation.

4.1.2. Chemical reactivity

FMO parameters (or global reactive descriptors), such $\Delta E = (E_{\text{HOMO}} - E_{\text{LUMO}})$, $I = -E_{\text{HOMO}}$, $A = -E_{\text{LUMO}}$, $\eta = (I - A)/2$, $\zeta = 1/2\eta$, $\chi = (I + A)/2$, $\mu = -(I + A)/2$, $\omega = \mu^2/2\eta$, and $\Delta N_{\text{max}} = -\mu/\eta$,

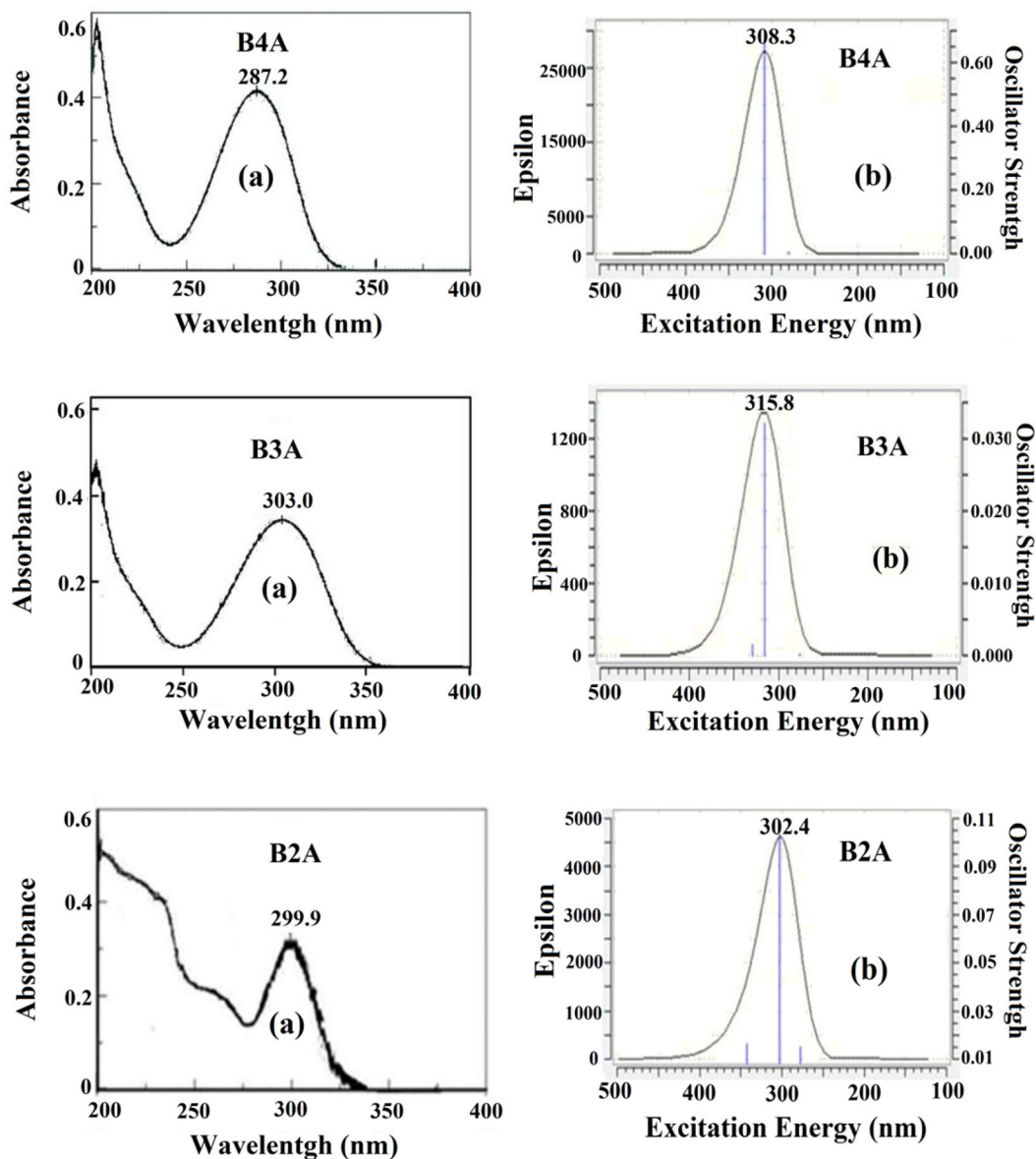


Figure 2. UV-Vis Spectra of B4A, B3A, and B2A: (a) Experimental (b) Simulated with TD-DFT/B3LYP 6-311++G(d,p) formalism.

Table 1. Electronic absorption parameters for B4A, B3A, and B2A as evaluated by TD-DFT/B3LYP/6-311++G(d,p) formalism.

Molecule	Absorption maximum λ_{\max} (nm)		Excitation energy (eV)	Oscillator strength (f)	Major contribution ($\geq 10\%$)	Transition
	Calculated	Experimental				
B4A	308.3	287.2	4.02	0.670	H _z →L (98%)	$\pi \rightarrow \pi^*$
B3A	315.8	303.0	3.92	0.031	H→L (88%)	$\pi \rightarrow \pi^*$
B2A	302.4	299.9	4.10	0.103	H→L (56%) H-1→L (15%) H-2→L (22%)	$\pi \rightarrow \pi^*$

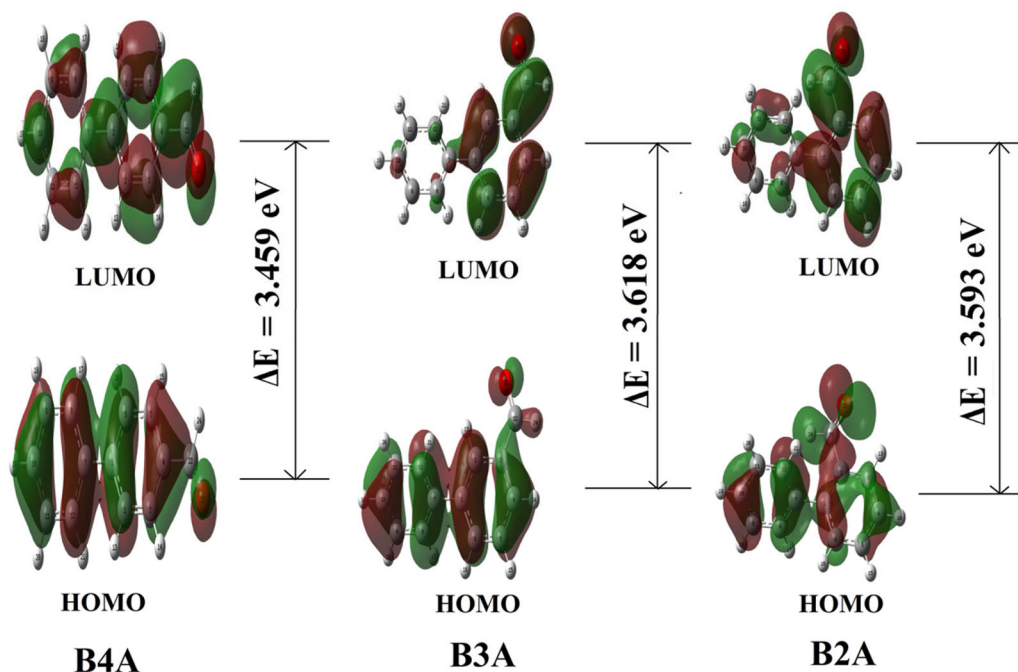


Figure 3. Frontier molecular orbitals of (a) B4A, (b) B3A, and (c) B2A as obtained using DFT/B3LYP/6–311++G(d,p) formalism.

Table 2. Frontier molecular orbital parameters of B4A, B3A, and B2A by DFT/B3LYP/6-311++G(d,p) method.

Frontier molecular orbital parameter	Value (eV)		
	B4A	B3A	B2A
HOMO energy	−9.781	−9.780	−9.795
LUMO energy	−6.322	−6.161	−6.200
Frontier molecular orbital energy gap	3.459	3.618	3.594
Ionization energy (I)	9.781	9.780	9.795
Electron affinity (A)	6.322	6.161	6.200
Global chemical hardness (η)	1.729	1.809	1.797
Global chemical softness (ζ)	0.289	0.276	0.278
Electronegativity (χ)	80.51	7.970	7.997
Chemical potential (μ)	−8.051	−7.970	−7.997
Global electrophilicity index (ω)	18.739	17.555	17.792
Maximum charge transfer index (ΔN_{\max}) ^a	4.656	4.406	4.450

^a ΔN_{\max} has no units as it is ratio of similar quantities

where estimated for B4A, B3A, and B2A on the basis of DFT/B3LYP/6-311++G(d,p) formalism.^{22,29–31} These are presented in Table 2. The primary quantity that can be obtained from these parameters is the energy gap, which is equal to the difference between orbital energies of HOMO and LUMO. This parameter, for B4A, B3A, and B2A, is calculated at 3.459, 3.619, and 3.595 eV, respectively, using the data from Table 2. These values are relatively small. This is a characteristics feature of conjugated molecules, and is an indicator of high chemical reactivity of B4A, B3A, and B2A. Low value of frontier orbital energy gap creates energetically favorable situation wherein it is easy to excite electrons from low-lying HOMO to high-lying LUMO leading to accumulation of electrons in the LUMO, polarizing the molecule. Thus a molecule having low energy gap is easily polarizable, has high chemical reactivity and exhibits low kinetic stability.^{47–49} From Table 2, we note that the

chemical potential (μ) for the three molecules under investigation is negative. This indicates that the molecules are stable under normal conditions.⁵⁰

4.2. Non-linear optical (NLO) properties

An electromagnetic wave, in its passage through a NLO material, experiences changes in its propagation characteristics, such as amplitude, frequency, or phase, due to its interaction with the material, generating new fields.^{51,52} If such modifications are sufficiently high, then the NLO material becomes useful for NLO applications, such as frequency shifting, optical logic, optical memory, and optical switching, in the fields of telecommuncations, signal processing, and optical inter-connections.^{22,50,52–56} First-order hyperpolarizability (β_t) plays a pivotal role in deciding the NLO behavior of a given material. Consequently, density functional formalism was extensively employed to investigate organic NLO materials.^{50–52,57–60}

The NLO quantities calculated for B4A, B3A, and B2A are collected in Table 3. Following usual practice one compares total molecular dipolemoment (μ_t) and total first-order hyperpolarizability (β_t) of a given material with values of corresponding quantities of urea, in order to evaluate NLO behavior of the material under consideration. For Urea μ_t and β_t are 1.3732 Debye and $372.8 \times 10^{-33} \text{ cm}^5/\text{esu}$, respectively. For B4A, the values of μ_t and β_t are 1.944 Debye and $4095.0427 \times 10^{-33} \text{ cm}^5/\text{esu}$, whereas the corresponding values for B3A are 1.674 Debye and $959.379 \times 10^{-33} \text{ cm}^5/\text{esu}$, while they are 1.445 Debye and $131.227 \times 10^{-33} \text{ cm}^5/\text{esu}$, for B2A. Thus, μ_t and β_t for B4A are 1.42 and 10.98 times of that of corresponding values for Urea.

Corresponding figures for B3A are 1.23 and 2.57, whereas they are 1.05 and 0.35 for B2A. Hence, B4A and B3A are very useful for NLO applications, whereas B2A is not useful for this purpose. The value of hyperpolarizability of a given material is a measure of NLO activity. Its origin is in the intramolecular charge transfer (ICT), which has its roots in electron cloud

Table 3. Values of dipole moment, μ_t (in Debye); polarizability, α_t (in $1.4818 \times 10^{-25} \text{ cm}^3$); and first-order hyperpolarizability, β_t (in $8.641 \times 10^{-33} \text{ cm}^5/\text{e.s.u}$) of B4A, B3A, and B2A.

Type of component	Value with B3LYP/6 – 311++G(d,p)		
	B4A	B3A	B2A
μ_x	1.766	–0.507	–0.592
μ_y	0.769	1.573	–1.313
μ_z	0.256	–0.264	0.108
μ_t	1.944	1.674	1.445
α_{xx}	325.930	275.444	209.787
α_{xy}	1.337	3.564	–5.408
α_{yy}	187.816	210.075	156.733
α_{xz}	–0.271	–4.720	3.764
α_{yz}	1.266	6.558	7.047
α_{zz}	108.889	111.662	100.801
α_t	207.545	199.060	155.774
$\Delta\alpha$	190.278	142.798	94.394
β_{xxx}	3886.314	630.762	146.142
β_{xxy}	125.307	–137.748	10.602
β_{xyy}	96.116	342.199	–68.437
β_{yyy}	109.183	–100.590	121.623
β_{xxz}	34.604	18.267	–16.502
β_{xyz}	38.461	–34.277	22.432
β_{yyz}	21.761	58.999	–55.422
β_{xzz}	103.982	–33.373	–7.823
β_{yzz}	20.648	50.142	–36.724
β_{zzz}	17.806	–30.739	15.208
β_t	4095.0427	959.379	131.227

association through π -conjugated structure of electrons. The components of hyperpolarizability decide charge delocalization in the molecule. In the case of B4A, B3A, and B2A, the direction along which maximum charge delocalization takes place is β_{xxx} direction.

4.3. Natural bond orbital (NBO) analysis

Results of important hyperconjugative interactions obtained with second-order perturbation theory analysis of Fock matrix in NBO basis using DFT/B3LYP/6-311++G(d,p) computational level for B4A, B3A, and B2A are summarized in Tables ST1, ST2, and ST3, respectively, which can be found in Supplementary information.

NBO method is a mathematical tool to construct orbitals so as to include maximum possible percentage of the ED. As a result, they are helpful in providing clear understanding of:

- i. ICT,
- ii. intra and intermolecular bonding interactions, and
- iii. hyperconjugative interactions between donor (i) and acceptor (j) groups within a given electronic structure.

To drive this point home let us consider the stabilization energy $E(2)$, associated with donor (i)→acceptor(j) electron delocalization, as estimated using the equation^{19,61}

$$E(2) = -q_i \frac{F_{ij}^2}{\Delta E} = -q_i \frac{\langle i|F|j \rangle^2}{\epsilon_j - \epsilon_i}$$

where q_i is the donor orbital occupancy, ϵ_i and ϵ_j are energies of i th and j th orbitals (diagonalelements), respectively, and F_{ij} is the off diagonal NBO Fock matrix element.

Significant value of stabilization energy $E(2)$ indicates strong interaction between the electron donors and electron acceptors resulting in greater extent of conjugation of the entire structure. The delocalization of ED, between occupied Lewis-type (bonding or lone pair) NBO orbitals and empty non-Lewis (anti-bonding or Rydberg) NBO orbitals implies stabilization of donor–acceptor interaction. Intramolecular hyper conjugative interactions arise due to overlap between the bonding π -orbitals and anti-bonding π^* -orbitals. This leads to ICT stabilizing the system. This type of interactions reveal themselves as enhancement in the ED in biphenyl C1–C6, C2–C3, C4–C5, C7–C12, C8–C9, and C10–C11 anti-bonding orbitals. They reduce strength of the corresponding bonds. The ED, for B4A at the conjugated π -bonds of the biphenyl ring is between 1.6159 and 1.6663, as can be seen from Table ST1, whereas the corresponding values, for π^* -anti-bonds are in the range 0.2688–0.3799. Consequent to this intense charge delocalization the molecule generates total stabilization energy 261.29 kcal mol⁻¹ from the biphenyl ring alone. The interactions π (C1–C6)→ π^* (C2–C3 and C4–C5); π (C2–C3)→ π^* (C1–C6 and C4–C5); π (C4–C5)→ π^* (C1–C6, C2–C3, and C22–O23); π (C7–C12)→ π^* (C8–C9 and C10–C11); π (C8–C9)→ π^* (C7–C12 and C10–C11); π (C10–C11)→ π^* (C7–C12 and C8–C9); LP(2) O23→ π^* (C4–C22) possess large stabilization energies in the range 17.68–24.12 kcal mol⁻¹, according to NBO analysis. As a result ICT, i.e. of π - electron movement from donor to acceptor (i.e. ICT) the molecule becomes more polarized. On the basis of this observation, it can be stated that the NLO properties of B4A originate from ICT. This statement substantiates the conclusion arrived at in Section Non-linear optical (NLO) properties on NLO properties, regarding the usefulness of the molecule for NLO applications. Corresponding conclusions can be arrived at for B3A and B2A from the data presented in Tables ST2 and ST3, respectively.

4.4. Molecular electrostatic potentials (MESP)

MESP is an established tool to understand molecular reactivity properties, by identifying electrophilic and nucleophilic regions, in addition to hydrogen bond interactions, in a molecule.⁶²⁻⁶⁴ The role of MESP extends to revealing nature of biological recognition processes. It also facilitates visual representation of relative polarities of a molecule. It is to be noted that MESP is a real physical quantity that can be measured with the help of diffraction experiments.^{65,66} This is an important aspect of MESP that distinguishes it from other reactivity indices like atomic charges that are mere defined properties, which do not correspond to anything real directly.

MESP maps obtained according to the formalism mentioned in Section Computational aspects, are available in Figure 4, for B4A, B3A, and B2A. It is customary to use color grading⁶⁷ to indicate regions of varying ED in the molecule. According to the color scheme, red indicates electron-rich region (partial negative charge); blue denotes electron deficient portion (partial positive charge); orange (light blue) gets associated with slightly electron deficient part (slightly less partial positive charge), yellow stands for slightly electron rich location (slightly less partial negative charge) and green identifies neutral area⁶¹ in a molecule. Hence the color grading from the most

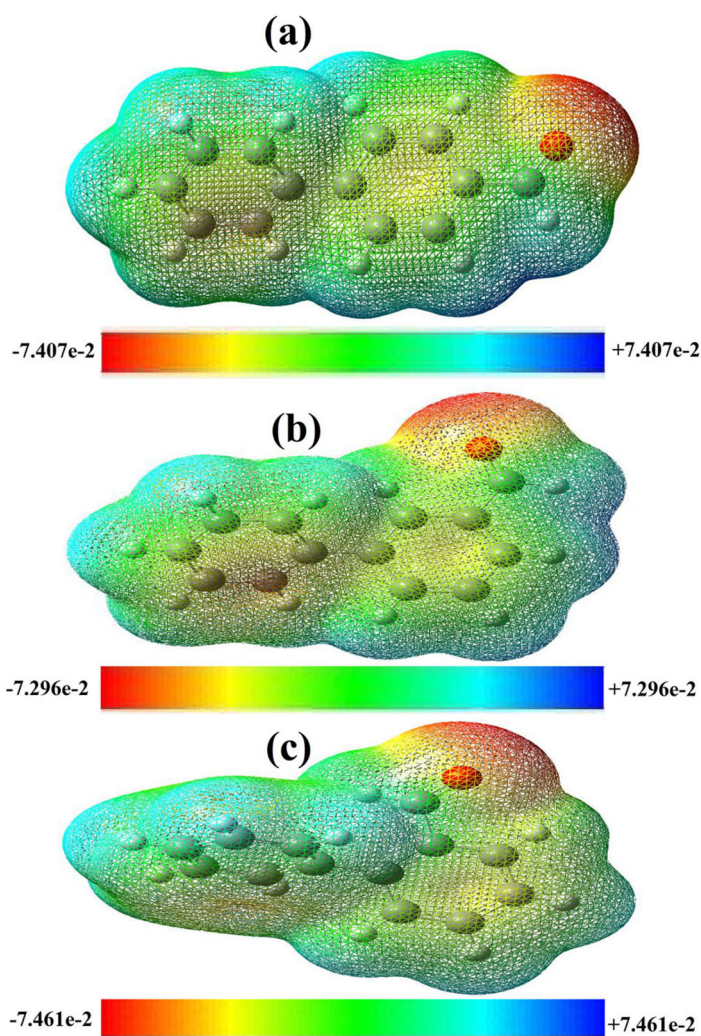


Figure 4. Total electron density mapped with electrostatic potential surface of (a) B4A, (b) B3A, and (c) B2A.

negative region to the highest positive region follows the order red > yellow > green > orange > blue. From Figure 4, it is clear that the highest electron-rich region in B4A contains oxygen atom of the aldehyde group. Hence, oxygen atom is the most reactive site in B4A. This is substantiated by the fact that this oxygen atom is involved in intermolecular hydrogen bond formation in B4A.¹⁷ These statements pertaining to B4A are equally true of B3A and B2A, as can be seen from Figure 4.

5. Conclusions

Theoretically simulated electronic transitions, one each for B4A, B3A, and B2A, at TD-DFT/B3LYP/6-311++G(d,p) level showed good agreement with their experimentally measured counterparts in a solution of CDCl₃ using IEF-PCM solution model. Their origin is in the $\pi \rightarrow \pi^*$ transitions in these molecules, as revealed by FMO (HOMO, LUMO) analysis. Global reactivity descriptors, such as energy gap (ΔE) and chemical potential (μ), evaluated through HOMO and LUMO analysis proved that the molecules are highly reactive attributable to relatively small value of corresponding energy gap, which is around 4 eV. Further, the negative value of related chemical potentials ascertained that the molecules were stable under normal conditions. The theoretical static NLO parameters μ_t and β_t of these molecules, on comparison with corresponding values of Urea, suggested that B4A and B3A were good for use in NLO industry, whereas such was not the case with B2A. Hyperconjugative interactions, as obtained from NBO, analysis, helped to explain NLO behavior of the molecules in terms of ICT. On the basis of MESP surface analysis by DFT, it was calculated that the most reactive site is located around the oxygen atom of aldehyde moiety in B4A, B3A, and B2A.

Acknowledgments

The authors sincerely acknowledge financial support, under SAP-DRS-II, extended by the University Grants Commission, New Delhi, India through their Lr.No.F.530/24/DRS-II, 2015 (SAP). They are also grateful to NIPER, Hyderabad for recording UV-Visible spectra. The first author (KSS) is grateful to the management of SR University, Warangal, India, for permitting him to undertake the reported investigations.

Disclosure statement

No potential conflict of interest was reported by the authors.

Funding

This work was supported under SAP-DRS-II, extended by the University Grants Commission, New Delhi, India through their Lr.No.F.530/24/DRS-II, 2015 (SAP).

ORCID

B. Venkatram Reddy  <http://orcid.org/0000-0001-6516-7731>

References

1. P. J. Collings, and M. Hird, *Introduction to Liquid Crystals Chemistry and Physics* (London: Taylor & Francis, 1997), 314. doi: [10.1201/9781315272801](https://doi.org/10.1201/9781315272801).
2. A. A. Patchett, and R. P. Nargund, "Chapter 26. Privileged Structures — an Update," *Annual Reports in Medicinal Chemistry* 35 (2000): 289–98.

3. H. Ji, M. Leung, Y. Zhang, K. J. Catt, and K. Sandberg, "Differential Structural Requirements for Specific Binding of Nonpeptide and Peptide Antagonists to the AT1 Angiotensin Receptor. Identification of Amino Acid Residues That Determine Binding of the Antihypertensive Drug Losartan," *Journal of Biological Chemistry* 269, no. 24 (1994): 16533–6.
4. W. J. Trotter, "Confirming Low Levels of Hexabromobiphenyl by Gasliquidchromatographyof Photolysis Products," *Bulletin of Environmental Contamination and Toxicology* 18, no. 6 (1977): 726–33.
5. R. Noyori, "Asymmetric Catalysis by Chiral Metal Complexes," *Chemtech (American Chemical Society)* 22, no. 6 (1992): 360–7.
6. C. Rosini, L. Franzini, A. Raffaelli, and P. Salvadori, "Synthesis and Applications of Binaphthyl C2-Symmetry Derivatives as Chiral Auxiliaries in Enantioselective Reactions," *Synthesis* 1992, no. 06 (1992): 503–17.
7. R. Schmid, J. Foricher, M. Cereghetti, and P. Schönholzer, "Axially Dissymmetric Diphosphines in the Biphenyl Series: Synthesis of (6,6'-Dimethoxybiphenyl-2,2'-Diyl)Bis(Diphenylphosphine)(MeO-BIPHEP) and Analogues via an ortho-Lithiation/Iodination Ullmann-Reaction Approach," *Helvetica Chimica Acta* 74, no. 2 (1991): 370–89.
8. F. P. GerhardBringmann, "Chapter 4 the Naphthylisoquinoline Alkaloids," *The Alkaloids: Chemistry and Pharmacology* 46 (1995): 127–271. doi: 10.1016/S0099-9598(08)60288-6.
9. D. H. Williams, and B. Bardsley, "The Vancomycin Group of Antibiotics and the Fight against Resistant Bacteria," *Angewandte Chemie International Edition* 38, no. 9 (1999): 1172–93. doi: 10.1002/(SICI)1521-3773(19990503)38:9 < 1172::AID-ANIE1172 > 3.0.CO;2-C.
10. P. J. Wagner, and B. J. Scheve, "Triplet Energy Transfer. 11. Steric Effects in the Singlet-Triplet Transitions of Methyl- and Chlorobiphenyls," *Journal of the American Chemical Society* 99, no. 9 (1977): 2888–92.
11. R. J. Pulham, and D. Steele, "Vibrational Spectra of 4, 4'-Difluorobiphenyl-d8 and the Structure of Biphenyls in Solution," *Journal of Raman Spectroscopy* 15, no. 4 (1984): 217–23. doi: 10.1002/jrs.1250150403.
12. X. Zhang, R. Xi, J. Liu, J. Jiang, G. Wang, and Q. Zeng, "Molecular and Electronic Structures as Well as Vibrational Spectra Assignment of Biphenyl, 2,2'- and 4,4'-Dichlorobiphenyl from Density Functional Calculations," *Journal of Molecular Structure: Theochem* 763, no. 1–3 (2006): 67–73. doi: 10.1016/j.theochem.2006.01.025.
13. Y. Takei, T. Yamaguchi, Y. Osamura, K. Fuke, and K. Kaya, "Electronic Spectra and Molecular Structure of Biphenyl and Para-Substituted Biphenyls in a Supersonic Jet," *The Journal of Physical Chemistry* 92, no. 3 (1988): 577–81. doi: 10.1021/j100314a003.
14. C. W. Lee, D. Pan, L. C. T. Shoute, and D. Lee Phillips, "Transient Resonance Raman Spectroscopic and ab Initio MO Investigation of Substituent Effects on the T1 Triplet States of Halobiphenyls," *Journal of Raman Spectroscopy* 32, no. 6–7 (2001): 461–70. doi: 10.1002/jrs.720.
15. M. K. Subramanian, P. M. Anbarasan, V. Ilangovan, and N. Sundaraganesan, "FT-IR, FT-Raman Spectra and DFT Vibrational Analysis of 2-Aminobiphenyl," *Molecular Simulation* 34, no. 3 (2008): 277–87. doi: 10.1080/08927020701829856.
16. K. Merkel, R. W. Rzalik, and A. Kocot, "Calculation of Vibrational Spectra for Cyanobiphenyl Liquid Crystals," *Journal of Molecular Structure* 563–564 (2001): 477–90. doi: 10.1016/S0022-2860(00)00891-7.
17. K. Srishailam, B. V. Reddy, and G. R. Rao, "Investigation of Torsional Potentials, Hindered Rotation, Molecular Structure and Vibrational Properties of Some Biphenyl Carboxaldehydes Using Spectroscopic Techniques and Density Functional Formalism," *Journal of Molecular Structure* 1196 (2019): 139–61. doi: 10.1016/j.molstruc.2019.06.064.
18. K. Srishailam, K. Ramaiah, K. Laxma Reddy, B. V. Reddy, and G. R. Rao, "Synthesis and Evaluation of Molecular Structure from Torsional Scans, Study of Molecular Characteristics Using Spectroscopic and DFT Methods of Some Thiosemicarbazones, and Investigation of their Anticancer Activity," *Chemical Papers* 75, no. 7 (2021): 3635–47. doi: 10.1016/j.molstruc.2008.06.031.
19. H. Gökce, S. Ceylan, N. Öztürk, and Y. Sert, "Tautomeric, Spectroscopic, Electronic and NLO Analyses of Purpald (4-Amino-3-Hydrazino-5-Mercapto-1,2,4-Triazole)," *Materials Today Communications* 32 (2022): 103862. doi: 10.1016/j.mtcomm.2022.103862.
20. G. A. El-Hitih, S. Q. Makki, Y. Sert, F. Uzun, M. B. Alshammari, P. Thordarson, and G. A. El-Hiti, "Synthesis, Spectrophotometric and DFT Studies of New Triazole Schiff Bases as Selective Naked-Eye Sensors for Acetate Anion," *Supramolecular Chemistry* 32 (2020): 519–26. doi: 10.1080/10610278.2020.1808217.
21. N. Dege, H. Gökce, O. E. Doğan, G. Alpaslan, T. Ađar, S. Muthu, and Y. Sert, "Quantum Computational, Spectroscopic Investigations on N-(2-((2-Chloro-4,5-Dicyanophenyl)Amino)Ethyl)-4-Methylbenzenesulfonamide by DFT/TD-DFT with Different Solvents, Molecular Docking and Drug-Likeness Researches," *Colloids and Surfaces A: Physicochemical and Engineering Aspects* 638 (2022): 128311. doi: 10.1016/j.colsurfa.2022.128311.

22. H. Gökce, Y. Sert, G. Alpaslan, A. S. El-Azab, M. M. Alanazi, M. H. M. Al-Agamy, and A. A.-M. Abdel-Aziz, "Hirshfeld Surface, Molecular Docking Study, Spectroscopic Characterization and NLO Profile of 2-Methoxy-4,6-Diphenylnicotinonitrile," *ChemistrySelect* 4 (2019): 9857–70. doi: [10.1002/slct.201902391](https://doi.org/10.1002/slct.201902391).
23. M. J. Frisch, *Gaussian 09 Revision B.01* (Wallingford CT: Gaussian, Inc, 2010).
24. A. D. Becke, "Density-Functional Thermochemistry. III. The Role of Exact Exchange," *The Journal of Chemical Physics* 98, no. 7 (1993): 5648–52.
25. C. Lee, W. Yang, and R. G. Parr, "Development of the Colle-Salvetti Correlation-Energy Formula into a Functional of the Electron Density," *Physical Review. B, Condensed Matter* 37, no. 2 (1988): 785–9.
26. D. Jacquemin, E. A. Perpète, I. Ciofini, and C. Adamo, "Accurate Simulation of Optical Properties in Dyes," *Accounts of Chemical Research* 42, no. 2 (2009): 326–34.
27. D. Jacquemin, J. Preat, V. Wathelet, M. Fontaine, and E. A. Perpète, "Thioindigo Dyes: Highly Accurate Visible Spectra with TD-DFT," *Journal of the American Chemical Society* 128, no. 6 (2006): 2072–83.
28. I. Ciofini, and C. Adamo, "Accurate Evaluation of Valence and Low-Lying Rydberg States with Standard Time-Dependent Density Functional Theory," *The Journal of Physical Chemistry A* 111, no. 25 (2007): 5549–56.
29. G. Gece, "The Use of Quantum Chemical Methods in Corrosion Inhibitor Studies," *Corrosion Science* 50, no. 11 (2008): 2981–92. doi: [10.1016/j.corsci.2008.08.043](https://doi.org/10.1016/j.corsci.2008.08.043).
30. K. Fukui, "Role of Frontier Orbitals in Chemical Reactions," *Science (New York, NY)* 218, no. 4574 (1982): 747–54.
31. R. G. Parr, L. V. Szentpály, and S. Liu, "Electrophilicity Index," *Journal of the American Chemical Society* 121, no. 9 (1999): 1922–4.
32. A. D. Buckingham, "Permanent and Induced Molecular Moments and Long-Range Intermolecular Forces," *Advances in Chemical Physics* 12 (1967): 107–40. doi: [10.1002/9780470143582.ch2](https://doi.org/10.1002/9780470143582.ch2).
33. E. D. Glendening, A. E. Reed, J. E. Carpenter, and F. Weinhold, *NBO Version 3.1* (Madison, WI: University of Wisconsin, 1998).
34. P. Politzer, P. R. Laurence, and K. Jayasuriya, "Structure-Activity Correlation in Mechanism Studies and Predictive Toxicology," *Environmental Health Perspectives* 61 (1985): 191–202.
35. C. Ho Choi, and M. Kertesz, "Conformational Information from Vibrational Spectra of Styrene, trans-Stilbene, and cis-Stilbene," *The Journal of Physical Chemistry A* 101, no. 20 (1997): 3823–31. no
36. R. G. Pearson, "Absolute Electronegativity and Hardness: Applications to Organic Chemistry," *The Journal of Organic Chemistry* 54, no. 6 (1989): 1423–30.
37. R. G. Parr, and R. G. Pearson, "Absolute Hardness: Companion Parameter to Absolute Electronegativity," *Journal of the American Chemical Society* 105, no. 26 (1983): 7512–6.
38. P. Geerlings, F. De Proft, and W. Langenaeker, "Conceptual Density Functional Theory," *Chemical Reviews* 103, no. 5 (2003): 1793–8731873.
39. C. G. Zhan, J. A. Nichols, and D. A. Dixon, "Ionization Potential, Electron Affinity, Electronegativity, Hardness, and Electron Excitation Energy: Molecular Properties from Density Functional Theory Orbital Energies," *The Journal of Physical Chemistry A* 107, no. 20 (2003): 4184–95.
40. R. M. Parrish, E. G. Hohenstein, P. L. McMahon, and T. J. Martínez, "Quantum Computation of Electronic Transitions Using a Variational Quantum Eigensolver," *Physical Review Letters* 122, no. 23 (2019): 230401.
41. D. Jacquemin, and E. A. Perpète, "Ab Initio Calculations of the Colour of Closed-Ring Diarylethenes: TD-DFT Estimates for Molecular Switches," *Chemical Physics Letters* 429, no. 1–3 (2006): 147–52. doi: [10.1016/j.cplett.2006.08.028](https://doi.org/10.1016/j.cplett.2006.08.028).
42. J. Preat, C. Michaux, A. Lewalle, E. A. Perpète, and D. Jacquemin, "Delocalisation in Conjugated Triazene Chromophores: Insights from Theory," *Chemical Physics Letters* 451, no. 1–3 (2008): 37–42. doi: [10.1016/j.cplett.2007.11.056](https://doi.org/10.1016/j.cplett.2007.11.056).
43. D. Maric, and J. P. Burrows, "Application of a Gaussian Distribution Function to Describe Molecular UV-Visible Absorption Continua. 1. Theory," *The Journal of Physical Chemistry* 100, no. 21 (1996): 8645–59.
44. D. Marić, J. N. Crowley, and J. P. Burrows, "Application of a Gaussian Distribution Function to Describe Molecular UV – Visible Absorption Continua. 2. The UV Spectra of RO2• Radicals," *The Journal of Physical Chemistry A* 101, no. 14 (1997): 2561–7.
45. É. A. G. Brémond, J. Kieffer, and C. Adamo, "A Reliable Method for Fitting TD-DFT Transitions to Experimental UV-Visible Spectra," *Journal of Molecular Structure: Theochem* 954, no. 1–3 (2010): 52–6. doi: [10.1016/j.theochem.2010.04.038](https://doi.org/10.1016/j.theochem.2010.04.038).
46. G. Scalmani, and M. J. Frisch, "Continuous Surface Charge Polarizable Continuum Models of Solvation. I. General Formalism," *The Journal of Chemical Physics* 132, no. 11 (2010): 114110.
47. L. Sinha, O. Prasad, V. Narayan, and S. R. Shukla, "Raman, FT-IR Spectroscopic Analysis and First-Order Hyperpolarisability of 3-Benzoyl-5-Chlorouracil by First Principles," *Molecular Simulation* 37, no. 2 (2011): 153–63. doi: [10.1080/08927022.2010.533273](https://doi.org/10.1080/08927022.2010.533273).

48. D. F. V. Lewis, C. Ioannides, and D. V. Parke, "Interaction of a Series of Nitriles with the Alcohol-Inducible Isoform of P450: Computer Analysis of Structure—Activity Relationships," *Xenobiotica* 24, no. 5 (1994): 401–408.
49. B. Kosar, and C. Albayrak, "Spectroscopic Investigations and Quantum Chemical Computational Study of (E)-4-Methoxy-2-[(p-Tolylimino)Methyl]Phenol," *Spectrochimica Acta. Part A, Molecular and Biomolecular Spectroscopy* 78, no. 1 (2011): 160–7.
50. M. Nakano, H. Fujita, M. Takahata, and K. Yamaguchi, "Theoretical Study on Second Hyperpolarizabilities of Phenylacetylene Dendrimer: Toward an Understanding of Structure–Property Relation in NLO Responses of Fractal Antenna Dendrimers," *Journal of the American Chemical Society* 124, no. 32 (2002): 9648–55.
51. Y. X. Sun, Q. L. Hao, W. X. Wei, Z. X. Yu, L. D. Lu, X. Wang, and Y. S. Wang, "Experimental and Density Functional Studies on 4-(3,4-Dihydroxybenzylideneamino)Antipyrine, and 4-(2,3,4-Trihydroxybenzylideneamino)Antipyrine," *Journal of Molecular Structure: Theochem* 904, no. 1–3 (2009): 74–82. doi: [10.1016/j.theochem.2009.02.036](https://doi.org/10.1016/j.theochem.2009.02.036).
52. Y. X. Sun, Q. L. Hao, W. X. Wei, Z. XueYu, L. D. Lu, X. Wang, and Y. S. Wang, "Experimental and Density Functional Studies on 4-(4-Cyanobenzylideneamino)Antipyrine," *Molecular Physics* 107, no. 3 (2009): 223–35.
53. C. Andraud, T. Brotin, C. Garcia, F. Pelle, P. Goldner, B. Bigot, and A. Collet, "Theoretical and Experimental Investigations of the Nonlinear Optical Properties of Vanillin, Polyvanillin, and Bisvanillin Derivatives," *Journal of the American Chemical Society* 116, no. 5 (1994): 2094–102. no
54. V. M. Geskin, C. Lambert, and J. L. Brédas, "Origin of High Second- and Third-Order Nonlinear Optical Response in Ammonio/Borato Diphenylpolyene Zwitterions: The Remarkable Role of Polarized Aromatic Groups," *Journal of the American Chemical Society* 125, no. 50 (2003): 15651–8.
55. D. Sajan, H. Joe, V. S. Jayakumar, and J. Zaleski, "Structural and Electronic Contributions to Hyperpolarizability in Methyl p-Hydroxy Benzoate," *Journal of Molecular Structure* 785, no. 1–3 (2006): 43–53. doi: [10.1016/j.molstruc.2005.09.041](https://doi.org/10.1016/j.molstruc.2005.09.041).
56. H. S. Nalwa, and S. Miyata, *Nonlinear Optics of Organic Molecules and Polymers* (Boca Raton, FL: CRC Press, 1997).
57. A. B. Ahmed, H. Feki, Y. Abid, H. Boughzala, C. Minot, and A. Mlayah, "Crystal Structure, Vibrational Spectra and Theoretical Studies of L-Histidinium Dihydrogen Phosphate-Phosphoric Acid," *Journal of Molecular Structure* 920, no. 1–3 (2009): 1–7.
58. J. P. Abraham, D. Sajan, V. Shettigar, S. M. Dharmaprakash, I. Nėmec, I. Hubert Joe, and V. S. Jayakumar, "Efficient π -Electron Conjugated Push-Pull Nonlinear Optical Chromophore 1-(4-Methoxyphenyl)-3-(3,4-Dimethoxyphenyl)-2-Propen-1-One: A Vibrational Spectral Study," *Journal of Molecular Structure* 917, no. 1 (2009): 27–36. doi: [10.1016/j.molstruc.2008.06.031](https://doi.org/10.1016/j.molstruc.2008.06.031).
59. S. G. Sagdinc, and A. Esme, "Theoretical and Vibrational Studies of 4,5-Diphenyl-2-2 Oxazole Propionic Acid (Oxaprozín)," *Spectrochimica Acta Part A, Molecular and Biomolecular Spectroscopy* 75, no. 4 (2010): 1370–6. no
60. A. Ben Ahmed, H. Feki, Y. Abid, H. Boughzala, and C. Minot, "Crystal Studies, Vibrational Spectra and Non-Linear Optical Properties of l-Histidine Chloride Monohydrate," *Spectrochimica Acta Part A, Molecular and Biomolecular Spectroscopy* 75, no. 1 (2010): 293–8.
61. F. Wienhold, and C. R. Landis, *Valency and Bonding-A Natural Bond Orbital Donor-Acceptor Perspective* (New York, NY: Cambridge University Press, 2005).
62. P. Politzer, and J. S. Murray, "The Fundamental Nature and Role of the Electrostatic Potential in Atoms and Molecules," *Theoretical Chemistry Accounts* 108, no. 3 (2002): 134–42.
63. L. F. Javier, L. J. Maria, and M. Orozco, "Electrostatic Interactions of a Solute with a Continuum. A Direct Utilization of ab Initio Molecular Potentials for the Prevision of Solvent Effects," *Theoretical Chemistry Accounts* 103 (2000): 343–5. doi: [10.1007/s002149900013](https://doi.org/10.1007/s002149900013).
64. I. V. Kochikov, Yu I. Tarasov, V. P. Spiridonov, G. M. Kuramshina, D. W. H. Rankin, A. S. Saakjan, and A. G. Yagola, "The Equilibrium Structure of Thiophene by the Combined Use of Electron Diffraction, Vibrational Spectroscopy and Microwave Spectroscopy Guided by Theoretical Calculations," *Journal of Molecular Structure* 567–568 (2001): 29–40.
65. J. Bentley, "Determination of Electronic Energies from Experimental Electron Densities," *The Journal of Chemical Physics* 70, no. 1 (1979): 159.
66. M. Fink, and R. A. Bonhan, "Electrostatic Potential of Free Molecules Derived from Electron Diffraction Results," *Chemical Applications of Atomic and Molecular Potentials* (1981): 93–122.
67. R. G. Pearson, "Absolute Electronegativity and Hardness Correlated with Molecular Orbital Theory," *Proceedings of the National Academy of Sciences of the United States of America* 83, no. 22 (1986): 8440–1.